5-20-2009

Proper Motions and Brightness Variations of Nonthermal X-Ray Filaments in the Cassiopeia a Supernova Remnant

Daniel J. Patnaude
Smithsonian Astrophysical Observatory

Robert A. Fesen
Dartmouth College

The Astrophysical Journal, 697:535–543, 2009 May 20 doi:10.1088/0004-637X/697/1/535

PROPER MOTIONS AND BRIGHTNESS VARIATIONS OF NONTHERMAL X-RAY FILAMENTS IN THE CASSIOPEIA A SUPERNOVA REMNANT

Daniel J. Patnaude[1] and Robert A. Fesen[2]
[1] Smithsonian Astrophysical Observatory, Cambridge, MA 02138, USA
[2] Department of Physics and Astronomy, 6127 Wilder Lab, Dartmouth College, Hanover, NH 03755, USA
Received 2008 August 5; accepted 2009 March 2; published 2009 May 4

ABSTRACT

We present *Chandra* ACIS X-ray observations of the Galactic supernova remnant Cassiopeia A taken in 2007 December. Combining these data with previous archival *Chandra* observations taken in 2000, 2002, and 2004, we estimate the remnant's forward shock velocity at various points around the outermost shell to range between 4200 and 5200 $\pm$ 500 km s^{-1}. Using these results together with previous analyses of Cas A's X-ray emission, we present a model for the evolution of Cas A and find that it's expansion is well fit by a $\rho_{\rm ej} \propto r^{-(7-9)}$ ejecta profile running into a circumstellar wind. We further find that while the position of the reverse shock in this model is consistent with that measured in the X-rays, in order to match the forward shock velocity and radius we had to assume that $\sim$ 30% of the explosion energy has gone into accelerating cosmic rays at the forward shock. The new X-ray images also show that brightness variations can occur for some forward shock filaments like that seen for several nonthermal filaments seen projected in the interior of the remnant. Spectral fits to exterior forward shock filaments and interior nonthermal filaments show that they exhibit similar spectra. This together with similar flux variations suggests that interior nonthermal filaments might be simply forward shock filaments seen in projection and not located at the reverse shock as has been recently proposed.

Key words: cosmic rays – ISM: individual (Cassiopeia A) – radiation mechanisms: non-thermal

Online-only material: color figures, mpeg animation

1. INTRODUCTION

Cassiopeia A (Cas A) is one of the youngest known Galactic supernova remnants (SNRs) with an estimated explosion date no earlier than 1681 $\pm$ 19 (Fesen et al. 2006). Optical echoes of the supernova outburst have been recently detected (Rest et al. 2008), the spectra of which indicate Cas A is the remnant of a Type IIb supernova event (Krause et al. 2008) probably from a red supergiant in the mass range of 15–25 $M_{\odot}$ that may have lost much its hydrogen envelope to a binary interaction (Young et al. 2006).

Viewed in X-rays, the remnant consists of a line emitting shell arising from reverse shocked ejecta rich in O, Si, Ar, Ca, and Fe (Fabian et al. 1980; Markert et al. 1983; Vink et al. 1996; Hughes et al. 2000; Willingale et al. 2002, 2003; Hwang & Laming 2003; Laming & Hwang 2003). Exterior to this shell are faint X-ray filaments which mark the current position of the remnant's forward shock front. The emission found here is nonthermal X-ray synchrotron radiation as well as faint line emission from shocked circumstellar material (CSM).

Vink et al. (1998) compared *Einstein* HRI to *ROSAT* HRI observations of Cas A to measure the expansion of the bright shell, finding an expansion age of $\sim$ 500 yr, considerably less than the $\sim$ 800 yr expansion age derived from 1.5 and 5.0 GHz radio observations (Anderson & Rudnick 1995), but similar to the 400–500 yr expansion age found by Agüeros & Green (1999) using data taken at 151 MHz. More recently, DeLaney & Rudnick (2003) using *Chandra* X-ray observations taken in 2000 and 2002 presented the first proper motion measurements of the forward blastwave velocity. Assuming a distance of 3.4 kpc (Reed et al. 1995), they estimated a blast wave expansion velocity of $\approx$ 5000 km s^{-1}.

Besides the outlying nonthermal emission filaments associated with the forward shock, some filamentary nonthermal X-ray emission is also seen in projection in the interior of the SNR (DeLaney et al. 2004). Whether these interior filamentary emissions originate from a wrinkled forward shock seen in projection or arises from nonthermal emission mechanisms in the interior of the SNR is currently uncertain (Laming 2001; Uchiyama & Aharonian 2008; Helder & Vink 2008).

Comparisons of *Chandra* observations taken in 2000, 2002, and 2004 revealed secular changes in several X-ray thermal knots and in one nonthermal filament projected in the remnant's interior (Patnaude & Fesen 2007). Uchiyama & Aharonian (2008) using the same multi-epoch *Chandra* observations found evidence for rapid variability in many more interior nonthermal X-ray emission filaments. Motivated by similar changes seen in RX J1713−3946 (Uchiyama et al. 2007), they measured the time variability of selected filaments to determine the local magnetic field strength in the variable regions. Their results suggest that the magnetic field in these regions is relatively high, B $\sim$ 1 mG.

Such a high magnetic field strength would be consistent with equipartition field strengths inferred in observations of bright radio knots in the remnant (Longair 1994; Wright et al. 1999). Uchiyama & Aharonian (2008) argue that their result points to a synchrotron origin for the emission coming from these knots, ruling out nonthermal bremsstrahlung from $\sim$ 100 keV electrons (Laming 2001), and suggest that this is strong evidence for a hadronic origin to the TeV emission observed in Cas A (Aharonian et al. 2001; Albert et al. 2007). Based on the location of the synchrotron knots, Uchiyama & Aharionian suggest that the emission is located primarily at the reverse shock, and Helder & Vink (2008) reach a similar conclusion.

Here we present forward shock velocity measurements using new *Chandra* ACIS observations of Cas A taken in 2007 December and compare these results to models for SNR evolution with and without efficient shock acceleration. The new observations show that many nonthermal emission filaments

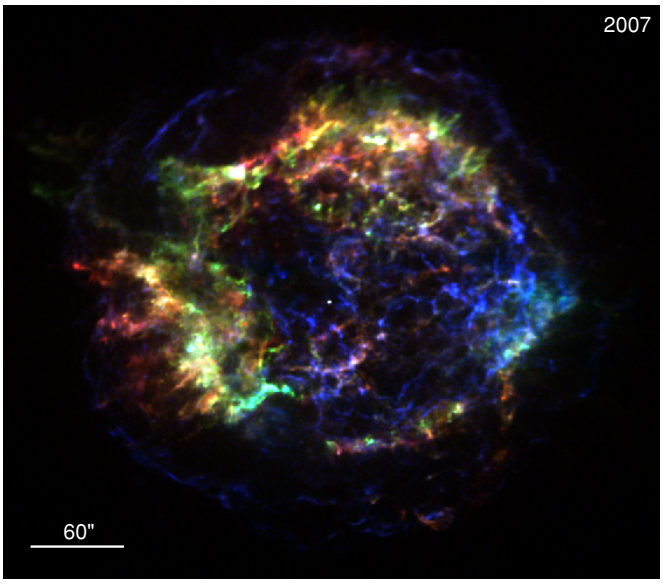

Figure 1. Exposure-corrected RGB color 2007 December image of Cas A. Red corresponds to 0.5–1.5 keV, green to 1.5–3.0 keV, and blue to 4.0–6.0 keV. This figure is part of the on-line animation, which shows the dynamical and spectral evolution of Cassiopeia A from 2000 January to 2007 December.

(A color version and an mpeg animation of this figure is available in the online journal.)

and features have undergone substantial brightness variations over the last four years. Model fits to the nonthermal emission coming from both the forward shock and the interior filaments indicate that they are quantitatively similar. We also present evidence for fast variability in forward shock front filaments which argues against the conclusion that rapid variability is a property restricted to emission at the reverse shock.

2. OBSERVATIONS

Cas A was observed with the ACIS-S3 chip on *Chandra* in two 25 ks observations taken on 2007 December 5 (ObsID 09117) and 2007 December 8 (ObsID 09773). The ACIS's 0.″492 CCD pixel scale undersamples the telescope's $\simeq$ 0.″5 resolution. The data were reprocessed using CIAO 4.0.1 and the latest version of the *Chandra* CalDB (Version 3.4.2). Figure 1 shows the combined, exposure-corrected image coded by energy. Red corresponds to 0.5–1.5 keV, green to 1.5–3.0 keV, and blue to 4.0–6.0 keV.

For our analyses, we also made use of previous *Chandra* ACIS observations taken on 2000 January 30 (ObsID 00114; PI: Holt), 2002 February 6 (ObsID 01952; PI: Rudnick), and 2004 February 8 (ObsID 05196; PI: Hwang). These archival data were also reprocessed using the latest version of the CalDB and all four ACIS images were projected to a common tangent point, chosen to be the expansion center determined by Thorstensen et al. (2001). Finally, the images were registered against the central compact object (CCO). Unregistered, the centroid of the Cas A CCO differs by 0.″08 between 2000 and 2002, and by 0.″33 between 2000 and 2008. We have registered the images against the year 2000 observations, though we note that when performing the same analysis on the unregistered images, we found no significant differences in our results.

To avoid the problems with bad columns and node boundaries discussed by DeLaney & Rudnick (2003), exposure corrected images for the 2000 and 2007 observations were created assuming a 1.85 keV source. We note that using a mono-energetic correction results in an artificially higher surface brightness for the forward shock filaments.

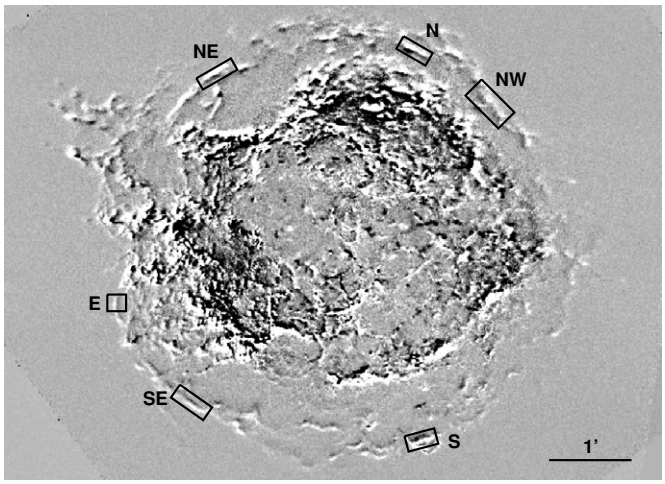

Figure 2. Difference image between 2000.08 and 2007.95 *Chandra* ACIS images. White correlates with the direction of filament motion. The boxes correspond to regions where we measured the filament proper motion.

3. RESULTS AND ANALYSIS

3.1. Proper Motion of the Forward Shock Front

Using the ACIS 2000 and 2002 images, DeLaney & Rudnick (2003) estimated the proper motions of several forward shock, nonthermal filaments around the SNR. Based on their average estimated proper motion of 0.″30 yr^{-1}, we expected the filaments to have shifted by $\simeq$ 2.″4 over 7.87 yr, or approximately five ACIS pixels. In a follow-up to their work, we used the locations of the forward shock X-ray filaments on our 2007 December ACIS images compared with their positions on 2000, 2002, and 2004 ACIS images to obtain improved estimates on the proper motion of the remnant's forward shock front.

Figure 2 shows a 2000 January–2007 December ACIS difference image of Cas A. The six labeled boxes correspond to regions where we measured the proper motions of the remnant's forward shock filaments. Figure 3 shows brightness profile plots of four forward shock filaments taken from the 2000.08 and 2007.95 ACIS images. As seen in Figure 3, there are relatively large and well defined positional separations between filament positions in the 2000 and 2007 data.

As noted by DeLaney & Rudnick (2003), a proper motion measurement using ACIS ideally should be done using images taken at the same telescope roll angle, as the telescope point-spread function (PSF) varies as a function of azimuthal angle. Unfortunately, the data taken in 2000 and 2007 are at different roll angles. To determine the effect that a varying PSF might have on our measurements, we modeled a 3 keV PSF at each of our chosen positions for the 2000 and 2007 observations. We found that at the average distance of 165″ from the nominal aimpoint of the observations, the telescope PSF varies by $\leqslant$ 0.″05, much less than an ACIS pixel and well below the average separations shown in Figure 3.

Filament positional shifts were measured two ways. We first fitted a Gaussian plus background model to the filament profiles and then measured the difference between the resulting Gaussian centroids. This method is not strictly accurate because the profiles for nonthermal filaments are not necessarily Gaussian but are shaped by the swept-up and compressed CSM/ISM

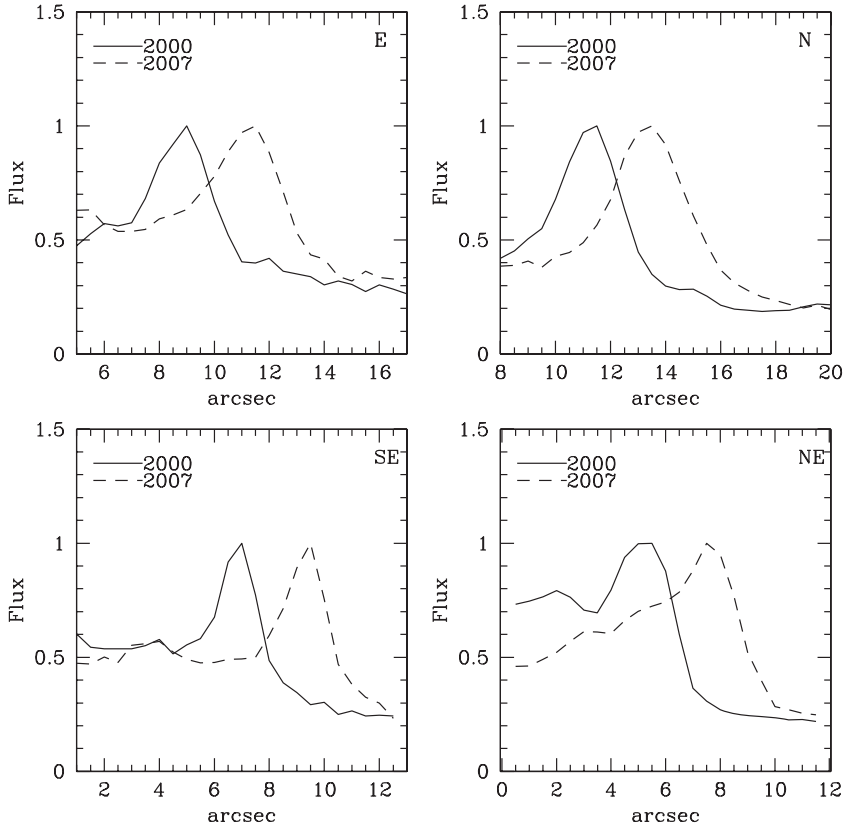

Figure 3. Nonthermal, forward shock filament emission profile plots are shown for four selected regions. Filament profiles from 2000 January and 2007 December are shown as solid and dashed lines, respectively.

Table 1
Forward Shock Filament Proper Motions

Region[a]	DeLaney & Rudnick (2003)[b]	Cross Correlation		Profile Fits	
		2000–2002	2000–2007	2000–2002	2000–2007
		($''$ yr^{-1})			
Southeast	$0\farcs38 \pm 0\farcs03$	$0\farcs31 \pm 0\farcs04$	$0\farcs31 \pm 0\farcs02$	$0\farcs33 \pm 0\farcs03$	$0\farcs32 \pm 0\farcs04$
East	$0\farcs38 \pm 0\farcs03$	$0\farcs30 \pm 0\farcs03$	$0\farcs31 \pm 0\farcs02$	$0\farcs30 \pm 0\farcs02$	$0\farcs32 \pm 0\farcs02$
Northeast	$0\farcs41 \pm 0\farcs02$	$0\farcs34 \pm 0\farcs04$	$0\farcs31 \pm 0\farcs04$	$0\farcs30 \pm 0\farcs04$	$0\farcs30 \pm 0\farcs03$
North	$0\farcs28 \pm 0\farcs01$	$0\farcs29 \pm 0\farcs03$	$0\farcs26 \pm 0\farcs02$	$0\farcs28 \pm 0\farcs03$	$0\farcs27 \pm 0\farcs02$
Northwest	...	$0\farcs25 \pm 0\farcs06$	$0\farcs27 \pm 0\farcs04$	$0\farcs28 \pm 0\farcs04$	$0\farcs28 \pm 0\farcs03$
South	...	$0\farcs31 \pm 0\farcs02$	$0\farcs32 \pm 0\farcs04$	$0\farcs32 \pm 0\farcs05$	$0\farcs34 \pm 0\farcs03$

Notes.
[a]The southeast, east, northeast, and north regions correspond to Regions 26, 29, 2, and 14, respectively in DeLaney & Rudnick (2003).
[b]Filament velocities from Table 2 of DeLaney & Rudnick (2003) and converted to proper motions assuming a distance of 3.4 kpc.

magnetic field and vary as a function of energy (Pohl et al. 2005). We also employed a cross-correlation technique to calculate filament shifts between the two epochs. This technique has been previously used in measuring proper motions of faint, thin Balmer-dominated filaments in the Cygnus Loop (see Patnaude & Fesen 2005 for details).

Table 1 lists our results for the six selected filament regions using both measurement techniques. Using the cross-correlation results, we estimate proper motions over the nearly eight year time span of 2000.08 to 2007.95 of $0\farcs26$ yr^{-1} to $0\farcs32$ yr^{-1} for the six regions around the SNR, with a typical 1σ error of $\pm 0\farcs03$ yr^{-1}.

In Table 1, we also list the 2000–2002 proper motion estimates reported by DeLaney & Rudnick (2003) along with our 2000–2002 measurements but using our measurement techniques. In general, we find smaller proper motions by some 15%–20%. In view that their quoted errors are comparable or even smaller than our measurements, we cannot easily account for these differences, but it may be related to the difference in how their analysis was performed. Since our results cover nearly four times the time span as their 2000.1–2002.1 proper motion estimates, our results should be more robust.

3.2. Cas A's Expansion Velocity and Deceleration

At a distance of 3.4 kpc, our measured proper range of $0\farcs26$–$0\farcs32$ yr^{-1} corresponds to forward shock front expansion velocities of $4200 - 5200 \pm 500$ km s^{-1}. The average expansion velocity for the six regions listed in Table 1 is ≈ 4900 km s^{-1}, in good agreement with the 5000 km s^{-1} reported by DeLaney & Rudnick (2003) for some two dozen regions.

Vink et al. (1998) measured the expansion of Cas A's main shell in X-rays by comparing *ROSAT* and *Einstein* HRI observations that were separated by 17 years. They found an expansion time-scale of 501 ± 15 yr, considerably more than the ≈325 yr optically derived age of Cas A (Thorstensen et al. 2001; Fesen et al. 2006), but also much less than the reported ∼ 800 yr expansion age determined in the radio (Anderson & Rudnick 1995), based on 1.5 and 5.0 GHz observations. Agüeros & Green (1999) found an expansion age similar to Vink et al. (1998), from 151 MHz observations.

Gotthelf et al. (2001) measured the angular size of Cas A to be 153″ ± 12″. Thorstensen et al. (2001) estimate an undecelerated explosion convergence date of 1671 ± 1 based on proper motion measurements on 17 outlying ejecta knots mainly using archival Palomar 5m images dating as far back as 1951, while Fesen et al. (2006) estimated a convergence date of 1681 ± 19 based on *HST* images for 126 knots covering a nine-month period which appear to be among the least decelerated ejecta. Based on these studies, we will adopt an explosion date of 1680, thus making the remnant's current age to be 329 yr.

This age yields a free expansion proper motion of 0.″465 yr^{-1}, or, assuming a distance of 3.4 kpc, a free expansion velocity of ≈ 7500 km s^{-1}. We can thus calculate the deceleration parameter of the blastwave as $m = (4900 \text{ km s}^{-1}/7500 \text{ km s}^{-1}) \approx 0.65$, or equivalently, using Gotthelf et al.'s angular remnant size in 2000, 0.″30 yr^{-1}/(153″ ± 12″ / 320 yr) ≈ 0.58–0.68.

3.3. Cas A Expansion Models

Our measurements of Cas A's forward shock proper motion and estimated deceleration parameter can be used to model the SNR's evolution. In ejecta-dominated remnants, the deceleration parameter is related to the self-similar evolution by $m = (n - 3)/(n - s)$ (Chevalier 1982; Truelove & McKee 1999; Laming & Hwang 2003), where n is the power-law index for the ejecta density profile ($\rho_{\rm ej} \propto r^{-n}$) and s is the power-law index for the ambient medium density profile ($\rho_{\rm amb} \propto r^{-s}$). Generally, $s = 0$ corresponds to a constant density ambient medium, while $s = 2$ corresponds to an ambient medium shaped by a circumstellar wind. For the progenitors of core-collapse SNe, such as Cas A, $s = 2$.

For remnants in the adiabatic (Sedov–Taylor) stage of expansion, the deceleration parameter $m = 0.67$. Many young remnants, such as Tycho, Kepler, SN 1006, and Cas A, are believed to be currently transitioning between the ejecta-dominated and Sedov stage. However, our calculated deceleration parameter of 0.65 is less than that expected for Sedov-type expansion, and corresponds to an ejecta power-law index of 4.85.

However, Laming & Hwang (2003) estimated a much higher ejecta density profile for Cas A. Using a Lagrangian hydrodynamics model coupled to a nonequilibrium ionization code, they self-consistently modeled the density profile of Cas A's expanding ejecta and found found that the ejecta density is well described by a power-law of index $n = 7$–9. This corresponds to a deceleration parameter of $m = 0.8$–0.86, considerably larger than our derived deceleration parameter of 0.65.

Truelove & McKee (1999) point out that for models for SNR evolution in which $3 < n < 5$, the bulk of the mass is concentrated at lower velocities, while the bulk of the energy is concentrated at higher velocities. Furthermore, the timescale by which a SNR enters the Sedov–Taylor phase of its evolution is set by the time that the reverse shock takes to travel through ejecta containing the bulk of the energy. Thus, in models with mass-poor and energy rich envelopes, this transition time can be very short. Laming & Hwang (2003) suggest that Cas A is currently transitioning from the ejecta-dominated to the Sedov–Taylor phase, so a power-law index as low as our estimated value of 4.85 seems unlikely.

In order to understand this discrepancy, we have tried to model Cas A's expansion. At an assumed distance of 3.4 kpc and a 320 yr age in 2000, Cas A's average forward shock radius of 153″ translates to 2.5 pc in radius and an average reverse shock radius 95″ ± 10″ corresponding to 1.6 ± 0.2 pc.

We adopted Laming & Hwang (2003) estimated explosion energy of 2×10^{51} erg and ejecta mass of 2 $M_\odot$, assume that the SNR is expanding into a red giant wind (Krause et al. 2008), and choose $v_{\rm wind} \approx 10$ km s^{-1} and $\dot{M} \approx 2 \times 10^{-5}$ $M_\odot$ yr^{-1}. The results of these adopted values, summarized in Model 1 in Table 2, show that our estimated ejecta power-law index of 4.85 does not reproduce the Cas A's measured parameters, producing a forward shock radius of 2.93 pc and velocity of 6300 km s^{-1} instead of the 2.5 pc and ≃5000 km s^{-1} values actually observed assuming a distance of 3.4 kpc.

Given that our initial derived ejecta power-law index does not agree with that derived from spectral fits to the SNR ejecta, we explored models with ejecta profiles consistent with Laming & Hwang's fits (Models 2–7 in Table 2). We note that a similar set of parameters were also chosen by Schure et al. (2008) in the context of Cas A's jet evolution in a Wolf–Rayet bubble, although their models do not consistently match both the observed blastwave radius and velocity either (see their Table 1).

As shown in Table 2, while our Models 2–7 may be appropriate for the evolution of the SNR ejecta and the jet, they overestimate the forward shock velocity regardless of choice of the power-law index of the ejecta or progenitor wind structure. These models also do not fit the measured expansion of Cas A, producing deceleration parameters of $m > 0.7$ and shock velocities $v_{\rm shock} > 5500$ km s^{-1}.

3.4. Cosmic Ray Acceleration at the Forward Shock

As there is a great deal of evidence suggesting that shocks in SNRs are efficient generators of cosmic rays (e.g., Warren et al. 2005), we then explored the inclusion of cosmic ray modification of the forward shock as a possible solution to these poor model fits. A signature of shock generated cosmic rays are nonthermal X-rays generated by synchrotron radiation due to shock-accelerated TeV electrons. High energy photons at GeV–Tev energies, either inverse Compton radiation from electrons or pion-decay emission from ions, have been detected from some SNRs including Cas A by HEGRA (Aharonian et al. 2001) and MAGIC (Albert et al. 2007).

In the production of cosmic rays, energy is removed from the SNR shock via particle acceleration. In doing so, the shock slows and the postshock gas becomes more compressed. We therefore also modeled Cas A under this assumption.

The inclusion of efficient acceleration at the forward shock should not alter the dynamics of the ejecta, and thus these models can be consistent with Laming & Hwang (2003). We also chose to only model shock acceleration at the forward shock. Although there have been suggestions that the bulk of the particle acceleration in Cas A might be occurring at the reverse shock (Uchiyama & Aharonian 2008; Helder & Vink 2008), the degree to which particle acceleration at the reverse shock is efficient remains an open question (see below).

Starting with the parameter space explored by Laming & Hwang (2003), we modeled Cas A assuming that some fraction of the explosion energy has gone into accelerating cosmic rays.

Table 2
Cas A Evolutionary Models

Model	M_{ej} ($M_\odot$)	E_{51} (10^{51} erg)	n	v_{wind} (km s^{-1})	$\dot{M}_{-5}$ (10^{-5} $M_\odot$ yr^{-1})	E(CR)/E(SN) (%)	R_{FS}	R_{RS}	V_{shock} (km s^{-1})	m
1	2	2	4.85	10	2	0	2.93	1.61	6300	0.70
2	2.5	2	9	5	1.5	0	2.44	1.42	5500	0.73
3	2	2	9	10	2	0	2.79	1.65	6376	0.74
4	2	2	8	10	2	0	2.78	1.67	6379	0.74
5	2	2	7	10	2	0	2.78	1.67	6390	0.74
6	2	2	6	10	2	0	2.78	1.73	6352	0.74
7	2	2	9	5	1.5	0	2.56	1.42	5679	0.72
8	2	2	9	10	2	7	2.73	1.67	6178	0.73
9	2	2	9	10	2	50	2.22	1.67	4613	0.67
10	2	2	9	10	2	17	2.64	1.67	5826	0.72
11	2	2	9	10	2	34	2.46	1.67	5021	0.66
12	2	2	8	10	2	34	2.46	1.67	5023	0.66
13	2	2	7	10	2	34	2.46	1.67	5033	0.66
14	2	2	9	10	1.5	27	2.68	1.85	5594	0.68
15	2	2	9	5	1.5	27	2.68	1.85	5594	0.68
16	2	1	9	10	2	0	2.14	1.36	5010	0.77
17	2	1.5	9	10	2	0	2.50	1.54	5768	0.76
18	1	1	9	10	2	0	2.40	1.17	5215	0.71
19	1.5	1	9	10	2	0	2.26	1.30	5120	0.74
20	1	1.5	9	10	2	0	2.77	1.30	5989	0.71
21	1.5	1.5	9	10	2	0	2.63	1.48	5861	0.73
22	2.5	1	9	4.7	1.5	0	1.88	1.17	4348	0.76
23	2.5	1.5	9	4.7	1.5	0	2.20	1.30	4994	0.74

These models were set up as in Ellison et al. (2007) where the nonlinear particle acceleration is tuned by an injection parameter which determines the fraction of thermal particles that are injected into the acceleration process thus determining how much of the energy of the SNR goes into cosmic rays. These models are listed as Models 8–15 in Table 2. The particle injection is sensitive to parameters such as the shock velocity and ambient density, so choosing a fixed injection while varying the environmental parameters will naturally lead to varying acceleration efficiencies, as seen in Models 14–15.

As expected and shown in Table 2, increasingly efficient particle acceleration leads to lower shock velocities and smaller forward shock radii, leading to smaller modeled expansion parameters. In Models 8–13, we attempted to tune the acceleration efficiency so as to match the measured forward shock expansion velocity and forward and reverse shock radii. We fixed the ejecta density distribution as well as the explosion and presupernova wind parameters, and in Models 11–13, we fixed the acceleration efficiency but varied the ejecta power-law index.

We found that Models 11–13, with power-law indices of $n = 7$–9, a wind velocity of v_{wind} of 10 km s^{-1}, and a progenitor pre-SN mass loss rate of $\dot{M} \approx 2 \times 10^{-5}\ M_\odot\ \mathrm{yr}^{-1}$ provide a good fit to our observations, where $\gtrsim 30\%$ of the SN explosion energy is lost in particle acceleration. This acceleration efficiency results in a modeled forward shock velocity of ~ 5000 km s^{-1}, forward and reverse shock radii of 2.46 pc and 1.67 pc, and a deceleration parameter of $m = 0.66$. These values agree well with our measured deceleration parameter of 0.65 and measured blastwave velocity of 4900 km s^{-1}, while also being consistent with the spectral fits of Laming & Hwang (2003) and the measured forward and reverse shock radii of 2.5 pc and 1.6 pc (Gotthelf et al. 2001). We found that varying the ejecta power-law index, has only a small effect on the final parameters, seen as a difference in the blastwave velocity in Models 11–13.

We also tried varying the presupernova wind parameters in Models 14–15 to match those of Schure et al. (2008). While these models result in similar deceleration parameters and forward shock radii to Models 11–13, they significantly overestimate the forward shock velocity.

Finally, in order to see if our results could be fit by models that do not include the effects of diffusive shock acceleration, we also explored a wider parameter space in both the ejecta mass and explosion energy. These are listed as Models 16–23 in Table 2, where in Models 16–21 we varied the explosion energy and ejecta mass between 1.0–2.0 $\times$ 10^{51} erg and 1.0–2.0 $M_\odot$. In Models 22–23, we only varied the explosion energy, while fixing the other parameters as in Model 2.

As seen in Table 2, varying the explosion energy and ejecta mass does not allow for a simultaneous fit of both the forward shock radius and velocity. For example, in Model 17 we find a suitable fit to the forward shock radius, but the reverse shock radius is too small and the forward shock velocity is too high. Conversely, in Models 16 and 19 the forward shock velocity is well fit, but the forward shock radius is too small. While it is conceivable that one could design a model which can simultaneously fit the forward shock radius and blastwave velocity, such a model might not be consistent with other parameters derived from spectral fits to the ejecta.

Although our modeling results suggest significant cosmic ray production at the forward shock, it is uncertain whether efficient particle acceleration might also be occurring at the reverse shock as well (Ellison et al. 2005). If efficient shock acceleration were occurring at the reverse shock, other effects of this acceleration would be directly observable, both in the dynamics of the reverse shock and in the emitted thermal spectrum (Ellison et al. 2005, 2007). Much like in shock acceleration at the forward shock, the process removes energy from the shock and softens the equation of state. If particle acceleration were efficient, we would expect to observe the reverse shock to be closer to the contact discontinuity (much like the forward shock is close to the contact discontinuity in Tycho's SNR; Warren et al. 2005). The fact that our cosmic ray models appear to predict with

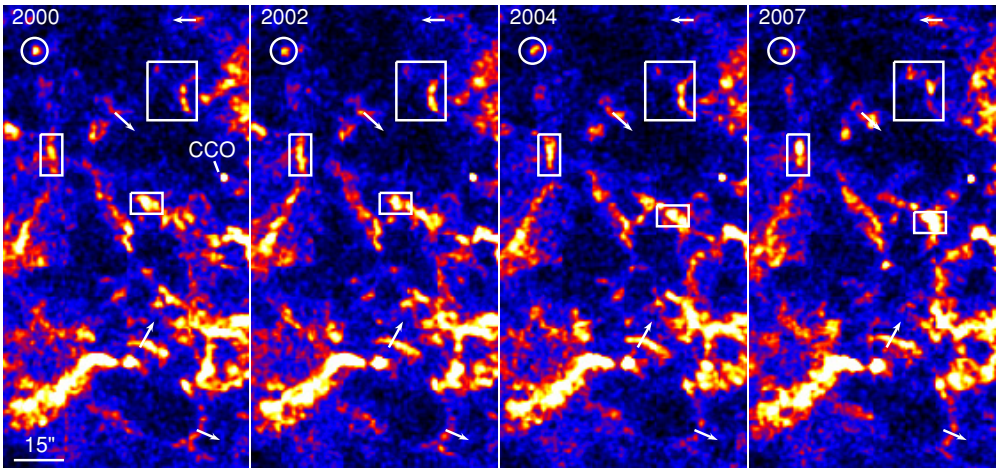

Figure 4. East-central region of Cas A in the 4.2–6.0 keV band. The four frames show the central region between 2000 and 2007. Boxes and the circle mark knots and filaments which show brightness variations along the filament, while arrows mark the location and direction of thin filaments which show proper motions between 2000 and 2007. The central compact object (CCO) is labeled for reference.

(A color version of this figure is available in the online journal.)

good accuracy the location of the reverse shock suggests that efficient acceleration may not be present at significant levels at the reverse shock. Furthermore, the presence of Fe–K emission at the reverse shock, seen in equivalent width maps (Hwang et al. 2000) suggests a high shock (and electron) temperature at the reverse shock, suggesting that the reverse shock has not lost much energy to cosmic ray acceleration.

3.5. Brightness Variations of Nonthermal X-ray Filaments and their Origin

Rapid changes in the brightness of thin, nonthermal filaments in the interior of Cas A have been noted previously via comparisons of the 2000–2004 observations (Patnaude & Fesen 2007; Uchiyama & Aharonian 2008). A comparison of all four epoch *Chandra* ACIS images, covering nearly an eight year time span, highlights and clarifies many of these changes in filament brightness and position. This is most readily seen in an on-line movie where we show the evolution of Cas A's X-ray emission between 2000 and 2007, of which Figure 1 is but one frame.

A close-up view of many of the changes exhibited by interior nonthermal emission features is presented in Figure 4, where we show the east-central region of Cas A in each epoch in the 4.2–6.0 keV band. In these images the remnant's global structure of continuum emission appears not unlike that seen in the radio; that is, the emission is characterized by thin, web-like and highly filamentary structures which often enclose patchy, faint diffuse emission.

A comparison of the four frames in Figure 4 reveals several regions where the continuum emission dramatically brightens or fades between 2000 January and 2007 December. Sections of some nonthermal filaments change so substantially between images that they resemble apparent rapid proper motions ($\simeq$ 0.″2–0.″3 yr^{-1}) that are, in some places, directed inward toward the remnant center or at some random, often nonradial direction. In addition, apparent sequential brightening of small sections of some filaments can give the appearance of motion along the filament.

Whereas the bulk of the changes in the remnant's nonthermal emission appear to come from knots and filaments which lie inside or projected onto the interior of the SNR, a few outer forward shock front filaments can also show similar changes in brightness. One filament associated with the forward shock, shown in Figure 5, shows evidence for substantial brightening between 2000 and 2007, with nonradial sequential changes seen along its length. This filament had previously been identified by Stage et al. (2006) as a potential site for efficient shock acceleration, and our new observations confirm that the filament exhibits behavior consistent with the changes seen in the interior filaments.

Uchiyama & Aharonian (2008) argue that emission flaring of nonthermal filaments is evidence for electron acceleration while a decrease in flux corresponds to synchrotron cooling. Using the *Chandra* ACIS 2000–2004 data, they found such emission flaring and fading was most apparent in interior filaments, leading them to conclude that such particle acceleration and synchrotron cooling was more likely to be occurring at the reverse shock, a conclusion supported by the deprojected continuum images of Cas A presented by Helder & Vink (2008).

However, the addition of the new 2007 December observations which increases the timespan from four to nearly eight years shows clear evidence for brightness variations of outer nonthermal filaments associated with the forward blastwave. As shown in Figure 5 and listed in Table 3, the northeast filament brightens substantially between 2004 January and 2007 December. Hence, rapid electron acceleration would appear to be occurring in some forward shock filaments as well.

In cases of increasing X-ray flux, the acceleration time of an X-ray emitting electron is given by $t_{\rm acc} \sim 9\eta B_{\rm mG}^{-3/2}\varepsilon_{\rm keV}^{1/2}V_{1000}^{-2}$ yr, where $\eta \geqslant 1$ is the electron gyro-factor, V_{1000} is the shock velocity in units of 1000 km s^{-1}, and $\varepsilon_{\rm keV}$ is the mean photon energy (≈ 1 keV). As listed in Table 1, the mean proper motion of this filament is $\sim 0.''30$ yr^{-1}, which at a distance of 3.4 kpc corresponds to $V_{1000} = 4.9$.

Uchiyama & Aharonian (2008) have suggested that such brightness changes in the remnant's interior nonthermal emission filaments originate at the remnant's reverse shock (due to their projected interior position), a notion first suggested by Bleeker et al. (2001) based on hardness ratios for interior and outer shock filaments as measured from *XMM-Newton* images. Support for the interpretation that the exterior and interior nonthermal emission filaments arise from different sources is the lack of radio emission associated with the exterior X-ray forward shock filaments, in contrast to the fair correlation that

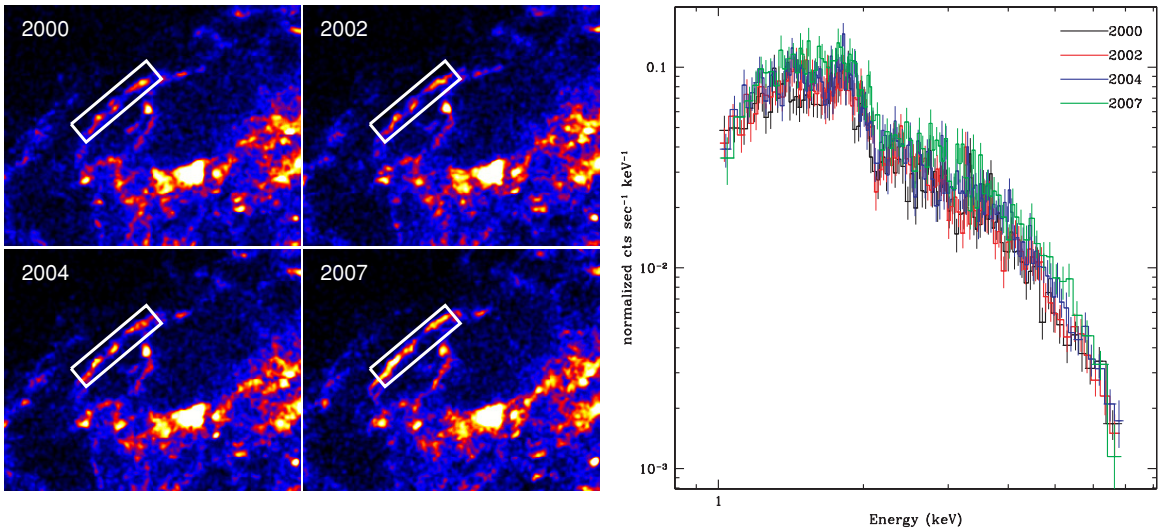

Figure 5. Left: exposure-corrected 4.2–6.0 keV images of a bright nonthermal filament (enclosed in the white box) in the northeast corner of Cas A. Right: spectral fits the spectrum from this filament. The fit results are listed in Table 3.

(A color version of this figure is available in the online journal.)

exists between interior radio and X-ray filaments (DeLaney 2004). Helder & Vink (2008) have also concluded that the interior nonthermal filaments originate from the reverse shock and not the forward shock.

On the other hand, DeLaney et al. (2004) and DeLaney (2004) have argued that interior nonthermal filaments may merely be forward shock filaments seen in projection against the face of Cas A. In this view, interior filamentary and web-like structures arise as the forward shock interacts with a lumpy, inhomogeneous CSM, with the observed brightness variations arising from line of sight tangencies of the shock front as it progresses through and around small CSM clouds and density variations.

We note that a correlation between global X-ray and radio filaments is not expected, thus undermining the meaning of any correlation of nonthermal radio and X-ray emitting features. Both Cassam-Chenaï et al. (2005) and Ellison & Cassam-Chenaï (2005) showed that in the remnants of core-collapse SNe interacting with a stellar wind, the nonthermal X-ray emission is strongly peaked at the shock front while radio emission will peak at the contact discontinuity. This can be seen in Figure 8 of Ellison & Cassam-Chenaï (2005) where the peak radio emissivity occurs well inside of the X-ray (see Figure 4 of Cassam-Chenaï et al. 2005 for another example).

To investigate the question of whether the nonthermal filaments projected in the interior of Cas A are associated with the reverse shock or the forward shock, we extracted spectra for six exterior forward shock filaments (including the northeast filament marked in Figure 5) and 23 interior projected nonthermal filaments from our 2007 December observations using the CIAO tool `specextract`. We also extracted spectra for these same filaments from the 2000, 2002, and 2004 data. These data were then fit with absorbed power laws. The results from these spectral fits for both exterior and interior filaments are listed in Table 3 and plotted in Figure 6.

Aside from obvious normalizations and differences in the absorbing column affecting the flux at lower energies, the spectra for exterior and interior nonthermal filaments are qualitatively quite similar (Figure 6). As shown in Table 3, while the fitted spectral indices hardly differ, interior filaments do appear to be marginally harder consistent with the conclusion of Bleeker et al. (2001).

Table 3
Nonthermal Filaments Spectral Fits

	Exterior Filaments[a]		Interior Filaments[b]		Northeast Filament[c]	
Epoch	Γ	1 keV Flux[d]	Γ	1 keV Flux[d]	Γ	1 keV Flux[d]
2000	$2.27^{+0.08}_{-0.08}$	$2.81^{+0.31}_{-0.28}$	$2.41^{+0.07}_{-0.07}$	$8.10^{+0.81}_{-0.73}$	$2.28^{+0.09}_{-0.08}$	$0.78^{+0.08}_{-0.08}$
2002	$2.27^{+0.07}_{-0.07}$	$3.31^{+0.32}_{-0.29}$	$2.41^{+0.06}_{-0.06}$	$8.59^{+0.81}_{-0.73}$	$2.39^{+0.08}_{-0.08}$	$0.96^{+0.10}_{-0.09}$
2004	$2.31^{+0.06}_{-0.06}$	$4.03^{+0.36}_{-0.33}$	$2.41^{+0.06}_{-0.06}$	$8.94^{+0.83}_{-0.75}$	$2.31^{+0.08}_{-0.08}$	$1.01^{+0.10}_{-0.09}$
2007	$2.35^{+0.08}_{-0.08}$	$5.15^{+0.57}_{-0.51}$	$2.36^{+0.07}_{-0.07}$	$10.1^{+0.11}_{-0.12}$	$2.29^{+0.09}_{-0.09}$	$1.18^{+0.13}_{-0.12}$

Notes.
[a]Galactic N_H fit at 1.15×10^{22} cm^{-2}.
[b]Galactic N_H fit at 2.01×10^{22} cm^{-2}.
[c]Galactic N_H fit at 1.22×10^{22} cm^{-2}.
[d]In units of 10^{-3} photons keV^{-1} cm^{-2} s^{-1}

3.6. Magnetic Field Strength

Lastly, we turn to the question of magnetic field strength in the filaments. As noted above, the northeast filament shows evidence for brightness changes over a nearly eight-year timespan. If we adopt an acceleration time $t_{\rm acc} \sim 2$–8 yr, then this corresponds to a magnetic field strength of $B_{\rm mG} \sim 0.1$–0.3, with the lower limit corresponding to the upper limit on the acceleration time. Our results are consistent with magnetic field strengths derived from previous observations (Longair 1994; Wright et al. 1999; Vink & Laming 2003; Atoyan et al. 2000; Berezhko & Völk 2004) as well as the recent results of Uchiyama & Aharonian (2008).

Recently, Bykov et al. (2008) simulated the effects of magnetic field turbulence on the observed synchrotron emission in young SNRs. They showed that the structure and evolution of small clumps ($\sim 10^{14}$–10^{16} cm) can change on timescales $\sim$ 1 yr. The angular size of the knots and filaments seen in Figure 4 is $\sim 5''$ which corresponds to $\sim 2.5 \times 10^{17}$ cm at Cas A's estimated a distance of 3.4 kpc. Significant flux variations on this spatial scale are seen to occur over the time period of

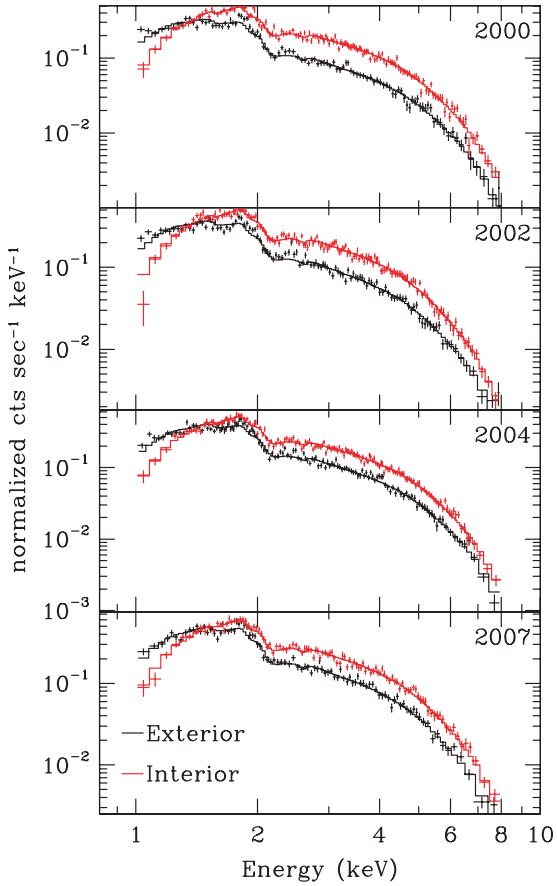

Figure 6. Extracted spectra for forward shock and interior nonthermal filaments. (A color version of this figure is available in the online journal.)

~ 4 yr, meaning that that yearly changes could occur over $\sim 6 \times 10^{16}$ cm.

Bykov et al. (2008) argue that intensity variations on such spatial scales are consistent with localized regions of high magnetic field ($\gtrsim 0.1$ mG), brought about by turbulence behind the shock. Furthermore, they point out that the integrated line of sight emissivity of these knots and filaments is what allows them to stand out against background emission. In Bykov et al. (2008), the shock is propagating perpendicular to the line of sight, but similar results are expected to be visible in face-on-shocks (A. M. Bykov 2009, private communication), consistent with our observations of flux changes seen in both the exterior and face-on filaments.

4. CONCLUSIONS

We have presented new *Chandra* ACIS observations of Cas A which were taken in late 2007. These new observations, when combined with previous *Chandra* data, allow us to constrain the velocity of the forward shock to be about 4900 km s^{-1}.

Combined with results from previous analyses of Cas A's X-ray emission (Laming & Hwang 2003; Gotthelf et al. 2001), we present several models for the evolution of Cas A and find that it's expansion can be well modeled by an $n = 7$–9 ejecta profile running into a circumstellar wind. We also find that the position of the reverse shock in this model is consistent with that measured by Gotthelf et al. (2001). However, in order to match the radius of the forward shock, we found that we must assume that the forward shock is efficiently accelerating cosmic rays.

Rapid changes in Cas A's synchrotron emission are seen for interior and exterior projected filaments, with both showing similar nonthermal spectra as well as inferred magnetic field strengths. Based on this and the simulations presented by Bykov et al. (2008), it is currently not clear whether the interior filaments are in fact located at the reverse shock as recently argued by Uchiyama & Aharonian (2008) and Helder & Vink (2008).

Instead, we propose that the interior filaments might be forward shocks seen in projection (DeLaney 2004). In that case, the observed brightness variations might arise from wrinkles in front-facing, forward shock as it moves through an inhomogeneous, local circumstellar medium.

Although we cannot rule out the possibility that interior nonthermal filaments are associated with the reverse shock, the combination of similar spectra, flaring timescale, and our fits to the remnant's dynamics are suggestive that the observed synchrotron flaring for interior filaments arises from forward shock filaments seen in projection toward Cas A's interior rather than at the reverse shock as recently suggested. At the least, our new X-ray data of Cas A shows that rapid brightness variations like those seen for interior nonthermal filaments can also be exhibited by some outer, nonthermal forward shock filaments.

We thank Don Ellison, Stephen Reynolds, and Martin Laming for many useful discussions during the preparation of this paper. We also thank the anonymous referee whose many suggestions and corrections significantly improved the paper. This work was supported by NASA grant GO8-9065A which is administered by the CXC at SAO. D.J.P. acknowledges support from NASA contract NAS8-39073.

Facilities: Chandra (ACIS).

REFERENCES

Agüeros, M. A., & Green, D. A. 1999, MNRAS, 305, 957
Aharonian, F., et al. 2001, A&A, 370, 112
Albert, J., et al. 2007, A&A, 474, 937
Anderson, M. C., & Rudnick, L. 1995, ApJ, 441, 307
Atoyan, A. M., Tuffs, R. J., Aharonian, F. A., & Völk, H. J. 2000, A&A, 354, 915
Berezhko, E. G., & Völk, H. J. 2004, A&A, 419, L27
Bleeker, J. A. M., Willingale, R., van der Heyden, K., Dennerl, K., Kaastra, J. S., Aschenbach, B., & Vink, J. 2001, A&A, 365, L225
Bykov, A. M., Uvarov, Y. A., & Ellison, D. C. 2008, ApJ, 689, L133
Cassam-Chenaï, G., Decourchelle, A., Ballet, J., & Ellison, D. C. 2005, A&A, 443, 955
Chevalier, R. A. 1982, ApJ, 258, 790
DeLaney, T., & Rudnick, L. 2003, ApJ, 589, 818
DeLaney, T., Rudnick, L., Fesen, R. A., Jones, T. W., Petre, R., & Morse, J. A. 2004, ApJ, 613, 343
De Laney, T. A. 2004, Ph.D. thesis, Univ. of Minnesota
Ellison, D. C., & Cassam-Chenaï, G. 2005, ApJ, 632, 920
Ellison, D. C., Decourchelle, A., & Ballet, J. 2005, A&A, 429, 569
Ellison, D. C., Patnaude, D. J., Slane, P., Blasi, P., & Gabici, S. 2007, ApJ, 661, 879
Fabian, A. C., Willingale, R., Pye, J. P., Murray, S. S., & Fabbiano, G. 1980, MNRAS, 193, 175
Fesen, R. A., et al. 2006, ApJ, 645, 283
Gotthelf, E. V., Koralesky, B., Rudnick, L., Jones, T. W., Hwang, U., & Petre, R. 2001, ApJ, 552, L39
Helder, E. A., & Vink, J. 2008, ApJ, 686, 1094
Hughes, J. P., Rakowski, C. E., Burrows, D. N., & Slane, P. O. 2000, ApJ, 528, L109
Hwang, U., Holt, S. S., & Petre, R. 2000, ApJ, 537, L119
Hwang, U., & Laming, J. M. 2003, ApJ, 597, 362
Krause, O., Birkmann, S. M., Usuda, T., Hattori, T., Goto, M., Rieke, G. H., & Misselt, K. A. 2008, Science, 320, 1195
Laming, J. M. 2001, ApJ, 563, 828

Laming, J. M., & Hwang, U. 2003, ApJ, 597, 347
Longair, M. S. 1994, High Energy Astrophysics (2nd ed.; Cambridge: Cambridge Univ. Press)
Markert, T. H., Clark, G. W., Winkler, P. F., & Canizares, C. R. 1983, ApJ, 268, 134
Patnaude, D. J., & Fesen, R. A. 2005, ApJ, 633, 240
Patnaude, D. J., & Fesen, R. A. 2007, AJ, 133, 147
Pohl, M., Yan, H., & Lazarian, A. 2005, ApJ, 626, L101
Reed, J. E., Hester, J. J., Fabian, A. C., & Winkler, P. F. 1995, ApJ, 440, 706
Rest, A., et al. 2008, ApJ, 681, L81
Schure, K. M., Vink, J., García Segura, G., & Achterberg, A. 2008, ApJ, 686, 399
Stage, M. D., Allen, G. E., Houck, J. C., & Davis, J. E. 2006, Nat. Phys., 2, 614
Thorstensen, J. R., Fesen, R. A., & van den Bergh, S. 2001, AJ, 122, 297
Truelove, J. K., & McKee, C. F. 1999, ApJS, 120, 299
Uchiyama, Y., & Aharonian, F. A. 2008, ApJ, 677, L105
Uchiyama, Y., Aharonian, F. A., Tanaka, T., Takahashi, T., & Maeda, Y. 2007, Nature, 449, 576
Vink, J., Bloemen, H., Kaastra, J. S., & Bleeker, J. A. M. 1998, A&A, 339, 201
Vink, J., Kaastra, J. S., & Bleeker, J. A. M. 1996, A&A, 307, L41
Vink, J., & Laming, J. M. 2003, ApJ, 584, 758
Warren, J. S., et al. 2005, ApJ, 634, 376
Willingale, R., Bleeker, J. A. M., van der Heyden, K. J., & Kaastra, J. S. 2003, A&A, 398, 1021
Willingale, R., Bleeker, J. A. M., van der Heyden, K. J., Kaastra, J. S., & Vink, J. 2002, A&A, 381, 1039
Wright, M., Dickel, J., Koralesky, B., & Rudnick, L. 1999, ApJ, 518, 284
Young, P. A., et al. 2006, ApJ, 640, 891